Version: April 4, 2018
Submitted to: EJMS Memorial Issue for Professor Rob Dunbar.

Formation and Reactions of the 1, 8-Naphthyridine (napy) Ligated Geminally-dimetallated Phenyl Complexes $[(napy)Cu_2(Ph)]^+$, $[(napy)Ag_2(Ph)]^+$ and $[(napy)CuAg(Ph)]^+$.†

Qiuyan Jin,[a] Jiaye Li,[a] Alireza Ariafard,[a,b] Allan J. Canty,[c] and Richard A. J. O'Hair*[a]

(a) School of Chemistry and Bio21 Institute of Molecular Science and Biotechnology, The University of Melbourne, Victoria 3010, Australia.

(b) Department of Chemistry, Faculty of Science, Central Tehran Branch, Islamic Azad University, Shahrak Gharb, Tehran, Iran

(c) School of Physical Sciences University of Tasmania Private Bag 75, Hobart, Tasmania 7001, Australia

* Corresponding Author:

E-mail: rohair@unimelb.edu.au

† Dedicated to the memory of our friend Prof. Rob Dunbar and in recognition of his important contributions to mass spectrometry and pioneering work on the spectroscopy of gas-phase ions.

Abstract:

Gas-phase ion trap mass spectrometry experiments and density functional theory (DFT) calculations have been used to examine the routes to formation of the 1,8-naphthyridine (napy) ligated geminally-dimetallated phenyl complexes $[(napy)Cu_2(Ph)]^+$, $[(napy)Ag_2(Ph)]^+$ and $[(napy)CuAg(Ph)]^+$ via extrusion of CO_2 or SO_2 under collision-induced dissociation (CID) conditions from their corresponding precursor complexes $[(napy)Cu_2(O_2CPh)]^+$, $[(napy)Ag_2(O_2CPh)]^+$, $[(napy)CuAg(O_2CPh)]^+$ and $[(napy)Cu_2(O_2SPh)]^+$, $[(napy)Ag_2(O_2SPh)]^+$, $[(napy)CuAg(O_2SPh)]^+$. Desulfination was found to be more facile than decarboxylation. DFT calculations reveal that extrusion proceeds via two transition states: **TS1** enables isomerization of the *O*,*O*- bridged benzoate to its *O*-bound form; **TS2** involves extrusion of CO_2 or SO_2 with concomitant formation of the organometallic cation and has the highest barrier. Of all the organometallic cations, only $[(napy)Cu_2(Ph)]^+$ reacts with water via hydrolysis to give $[(napy)Cu_2(OH)]^+$, consistent with DFT calculations which show that hydrolysis proceeds via the initial formation of the adduct $[(napy)Cu_2(Ph)(H_2O)]^+$ which then proceeds via **TS3** in which the coordinated H_2O is deprotonated by the coordinated phenyl anion to give the product complex $[(napy)Cu_2(OH)(C_6H_6)]^+$, which then loses benzene.

Keywords: Metal carboxylates, decarboxylation, metal sulfinates, desulfination, organocopper and organosilver, gas phase, mass spectrometry, DFT calculations.

Introduction:

Copper and silver aryls play important roles in organic synthesis, either as stoichiometric reagents or as reactive intermediates in catalytic cycles.[1] Examples of the former include Gilman reagents[2] and mesityl copper[3], while examples of the latter include the Ullman reaction[4] as well as copper and silver catalyzed protodecarboxylation reactions[5] and decarboxylative coupling reactions[6]. X-ray crystallographic studies[7] have revealed that copper and silver aryls exhibit diverse structures ranging from mononuclear "ate" complexes[8] (Scheme 1A) to oligomeric structures, which typically involve an aryl group bridging between two metal centers. Examples of the latter include: anionic, neutral and cationic dimers[9,10] (Schemes 1B and C); the copper trimer cation $[Cu_3Ph_2(PMDTA)_2]^+$ (PMDTA = *N,N,N′,N″,N″*-pentamethyldiethylenetriamine)[11]; copper and silver tetramers[12,13] (Scheme 1D); neutral and anionic ("ate") pentamers[11,12,14] (Scheme 1E); hexamers[15]; and octamers[16]. The bonding arrangement in these oligomers typically involves two-electron three-center bonding as exemplified for the $PhCu_2$ subunit in Scheme 1F,

with contribution **6a** involving the combination of the C(sp^2) molecular orbital of the bridging aryl group with a mutually bonding combination of Cu orbitals[17,18].

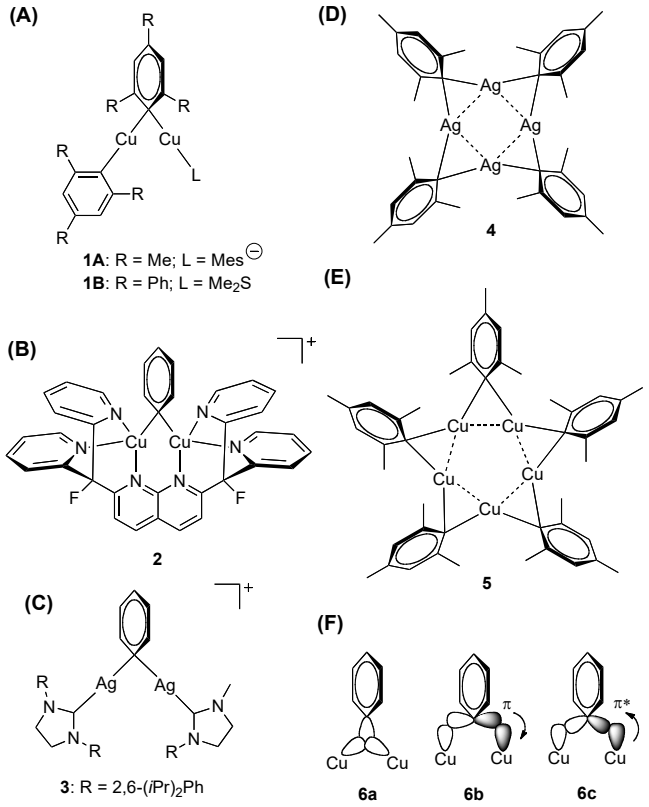

Scheme 1: Structures of copper aryls: **(A)** binuclear cuprates and neutral complexes[9]; **(B),(C)** ligated cationic dimers[10]; **(D)** tetramer[11]; **(E)** pentamer[11]. **(F)** Orbital description of two-electron three-center bonding[15].

Multistage mass spectrometry experiments[19] have been used to prepare and examine the reactivity of binuclear coinage metal organometallic cations, including the "bare" systems $[CH_3Cu_2]^+$, $[CH_3Ag_2]^+$, $[CH_3CuAg]^+$ [20], $[RCCAg_2]^+$ [21], $[PhAg_2]^+$ [22], and the "ligated" systems $[(dppm)Au_2(Ph)]^+$ [23]. We recently examined the role of substituents in the decarboxylation of 25 different coordinated aromatic carboxylates in binuclear complexes, $[(napy)Cu_2(O_2CC_6H_4X)]^+$, where napy = 1,8-naphthyridine [24,25] and X = H and the *ortho (o)*, *meta (m)* and *para (p)* isomers of F, Br, CN, NO_2, CF_3, OAc, Me and MeO. Although the substituents on the aryl group were found to influence the branching ratios (BR) of the product channels, decarboxylation to yield the organometallic cation $[(napy)Cu_2(C_6H_4X)]^+$ was always found to be the dominant pathway. Here we examine routes to the formation of the related ligated binuclear phenyl cations $[(napy)Cu_2(Ph)]^+$, $[(napy)Ag_2(Ph)]^+$, and $[(napy)CuAg(Ph)]^+$ via the collision-induced dissociation (CID) fragmentation of coordinated carboxylate or sulfinate ligands[26] and the subsequent unimolecular and ion-

molecule reactions of these organometallic cations with water[27]. Scheme 2 shows the systems examined and gives the numbering associated with likely intermediates associated with the extrusion reactions.

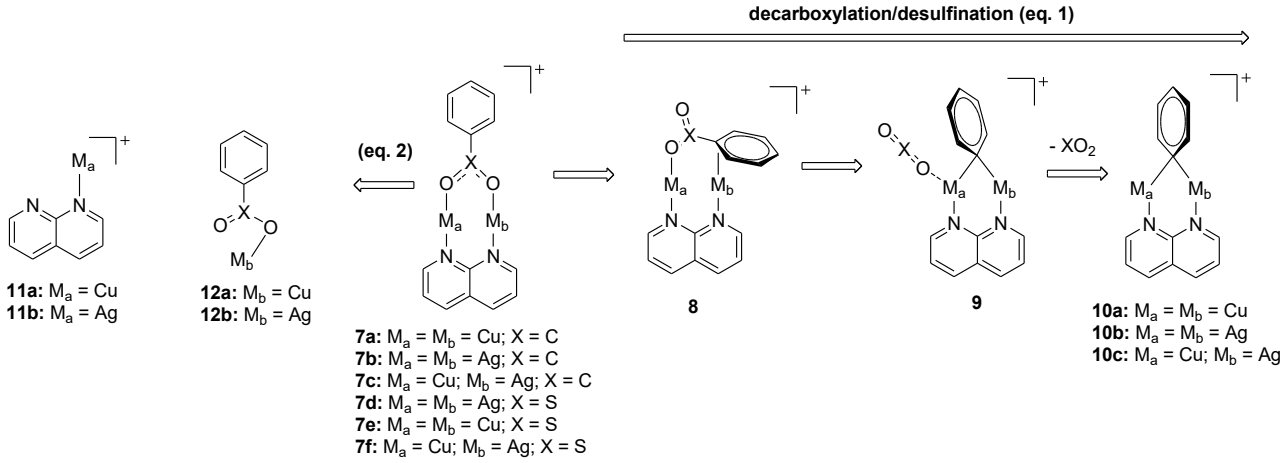

Scheme 2: Key species examined in this work.

Results and Discussion

1 Gas-phase formation of $[(napy)Cu_2(Ph)]^+$, $[(napy)Ag_2(Ph)]^+$ and $[(napy)CuAg(Ph)]^+$.

The thermal extrusion of CO_2 and SO_2 from coordinated carboxylates and sulfinates has been widely used to synthesize organometallics in both the condensed[28] and gas phase[19,29] and forms the basis of a range of metal catalyzed cross coupling reactions in organic synthesis[30,31]. The desired precursor complexes, $[(napy)M_aM_b(O_2XPh)]^+$ (**7a-7f**), were prepared by positive ion electrospray ionization of methanolic solutions of a mixture of a metal salt (copper(I) acetate or silver(I) nitrate), the napy ligand together with either benzoic acid or sodium benzenesulfinate. These complexes, which exhibited the expected *m/z* and isotope patterns associated with their formulations, were mass selected and subjected to low energy CID with the helium bath gas of the ion trap mass spectrometer (Figure 1). In all cases decarboxylation or desulfination of the coordinated carboxylates and sulfinates (eq. 1, Scheme 2) to yield the desired organometallic cation, $[(napy)M_aM_b(Ph)]^+$ (**10a-10c)**, was in competition with loss of a metal carboxylate or metal sulfinate (eq. 2, Scheme 2) to give mononuclear species **(11a,11b**), [32] where major products only are shown in Figure 2. With the exception of CID of $[(napy)Ag_2(O_2CPh)]^+$ (Figure 1B), the organometallic cation, $[(napy)M_aM_b(Ph)]^+$ is the base peak in the CID spectrum.

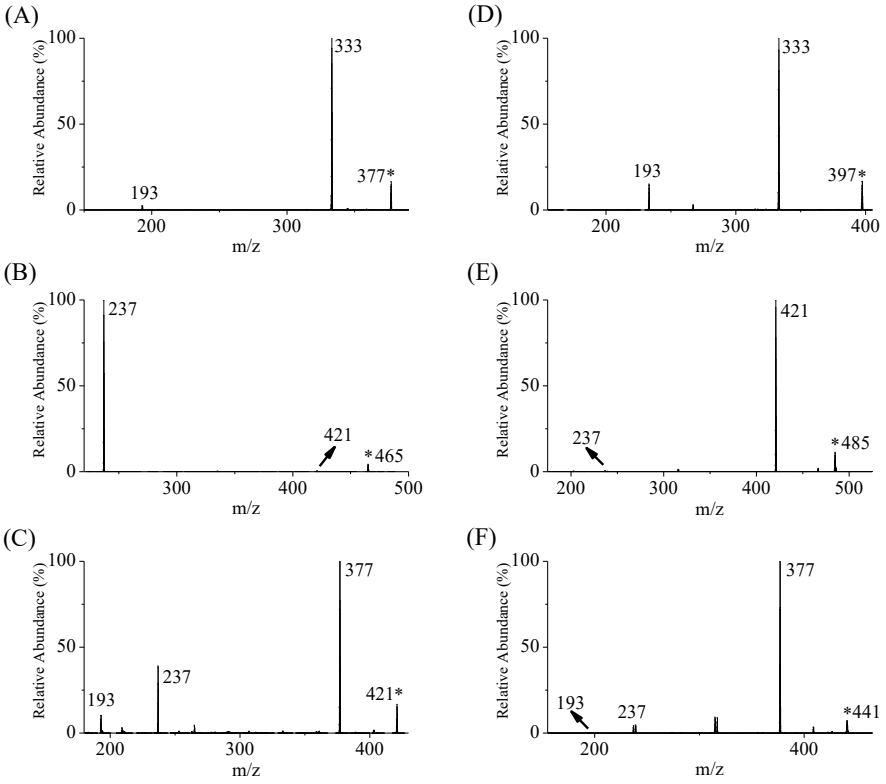

Figure 1: LTQ low energy CID mass spectra obtained using a Q value of 0.25 and an activation time of 30 ms with the given normalized collision energies (NCE) for the following species: **(A)** $[(napy)Cu_2(O_2CPh)]^+$, **7a** *m/z* 377 (NCE = 20%); **(B)** $[(napy)Ag_2(O_2CPh)]^+$, **7b** *m/z* 465 (NCE = 10%); **(C)** $[(napy)CuAg(O_2CPh)]^+$, **7c** *m/z* 421 (NCE = 15%); **(D)** $[(napy)Cu_2(O_2SPh)]^+$, **7d** *m/z* 397 (NCE = 16.5%); **(E)** $[(napy)Ag_2(O_2SPh)]^+$, **7e** *m/z* 485 (NCE = 8%); **(F)** $[(napy)CuAg(O_2SPh)]^+$, **7f** *m/z* 441 (NCE = 10%). * represents the monoisotopic peaks corresponding to ^{63}Cu, ^{107}Ag and ^{32}S isotopes that were mass selected.

We next carried out energy resolved collision-induced dissociation (ERCID) [33] to further investigate the transformation of $[(napy)M_aM_b(O_2XPh)]^+$ (**7a-7f**) to the organometallic cations $[(napy)M_aM_b(Ph)]^+$ (**10a-10c**). Under the ERCID condition, decarboxylation of **7a** and desulfination of **7d** yielded $[(napy)Cu_2(Ph)]^+$ as the main product, which is evidenced by the steady increase of their abundance with increasing depletion of the precursor ion. A small portion (~ 5%) of $[(napy)Cu]^+$ was also produced. Formation of $[(napy)Ag]^+$ is a significant channel in the ERCID of $[(napy)Ag_2(O_2CPh)]^+$ and $[(napy)CuAg(O_2CPh)]^+$, whereas the formation of $[(napy)Cu]^+$ was only a minor channel for $[(napy)Cu_2(Ph)]^+$ and $[(napy)AgCu(Ph)]^+$. Unlike guided ion beam experiments[34], it is not possible to determine accurate activation energies for the fragmentation channels[35]. However, using a crude approximation of 50% depletion (by relative abundance) of the precursor ion[35b] as shown by the dashed lines in Figure 2, the relative ease of fragmentation of the precursor ions follows the order: $[(napy)Cu_2(O_2SPh)]^+$

≈ $[(napy)Ag_2(O_2SPh)]^+$ ≈ $[(napy)CuAg(O_2SPh)]^+$ > $[(napy)Ag_2(O_2CPh)]^+$ > $[(napy)CuAg(O_2CPh)]^+$ ≈ $[(napy)Cu_2(O_2CPh)]^+$. Thus fragmentation of the coordinated sulfinates via desulfination is more facile than fragmentation of the benzoate complexes, which is consistent with a previous study on the relative ease of fragmentation of carboxylates versus sulfinates coordinated to a copper center in mononuclear cuprates[29].

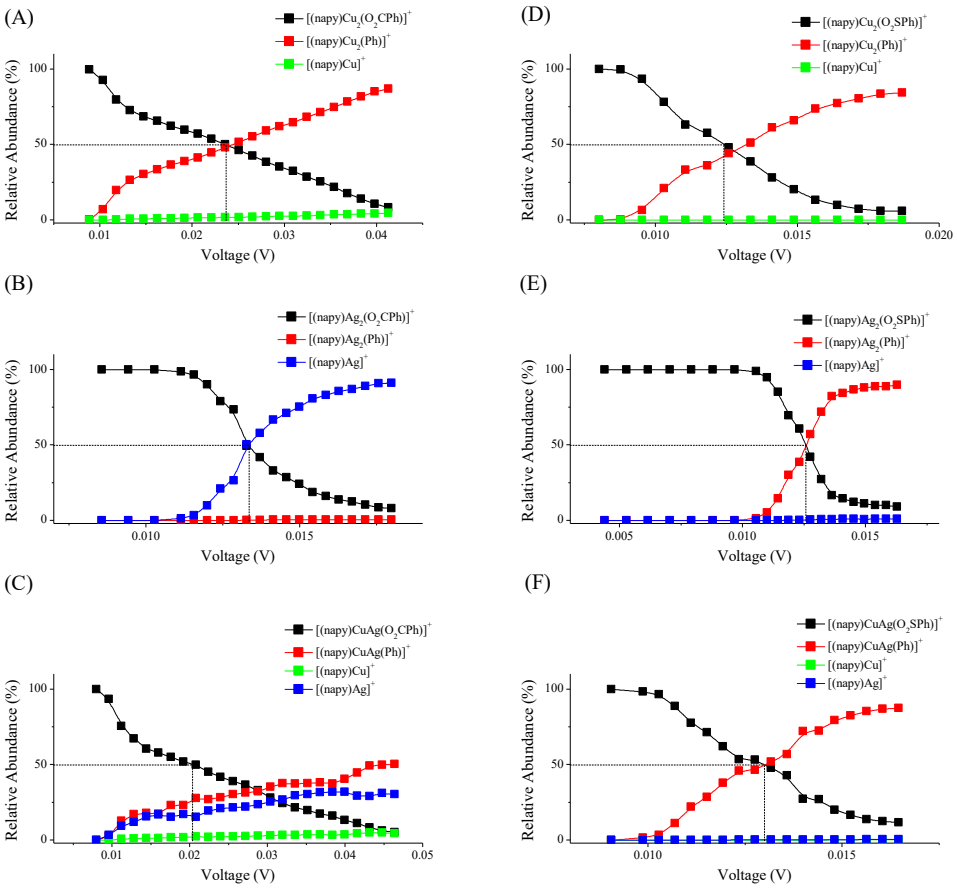

Figure 2: Energy resolved collision-induced dissociation mass spectra: **(A)** $[(napy)Cu_2(O_2CPh)]^+$, **7a** *m/z* 377; **(B)** $[(napy)Ag_2(O_2CPh)]^+$, **7b** *m/z* 465; **(C)** $[(napy)CuAg(O_2CPh)]^+$, **7c** *m/z* 421; **(D)** $[(napy)Cu_2(O_2SPh)]^+$, **7d** *m/z* 397; **(E)** $[(napy)Ag_2(O_2SPh)]^+$, **7e** *m/z* 485; **(F)** $[(napy)CuAg(O_2SPh)]^+$, **7f** *m/z* 441. Monoisotopic peaks corresponding to ^{63}Cu, ^{107}Ag and ^{32}S isotopes were mass selected. Spectra were obtained using the LTQ mass spectrometer. A Q of 0.25 and an activation time of 10 ms were used. The activation voltages for 50% depletion (by relative abundance) of the precursor ion as shown by the dashed lines are given. {$[(napy)Cu_2(O_2CPh)]^+$ (0.0237V); $[(napy)Ag_2(O_2CPh)]^+$ (0.0133V); $[(napy)CuAg(O_2CPh)]^+$ (0.0203V); $[(napy)Cu_2(O_2SPh)]^+$ (0.0124V); $[(napy)Ag_2(O_2SPh)]^+$ (0.0126V); $[(napy)CuAg(O_2SPh)]^+$ (0.0130V)}

2 Gas-phase fragmentation of $[(napy)Cu_2(Ph)]^+$, $[(napy)Ag_2(Ph)]^+$ and $[(napy)CuAg(Ph)]^+$.

Since organometallic compounds can undergo thermal decomposition[36], we have been examining the fundamental gas phase unimolecular decomposition reactions of organometallic ions[21b,22,37]. The CID channels for organocuprates and organoargentates $[RMCH_3]^-$ (M = Cu and Ag) have been studied in detail[37a,b], and are sensitive to the nature of both the R group and the metal, M. $[PhCuCH_3]^-$ and $[PhAgCH_3]^-$ both fragment mainly via bond homolysis (eq. 3a), with phenide formation (eq. 3b) being only a minor channel. Only $[PhCuCH_3]^-$ undergoes a minor amount of fragmentation via a dyotropic rearrangement (eq. 3c). Finally CID of $PhAg_2^+$ proceeds via the exclusive formation of Ag^+ (eq. 4)[22].

$$[PhMCH_3]^- \rightarrow [PhM]^{-\bullet} + CH_3^\bullet \quad (3a)$$

$$\rightarrow Ph^- + CH_3M \quad (3b)$$

$$\rightarrow PhCH_2^- + MH \quad (3c)$$

$$PhAg_2^+ \rightarrow Ag^+ + PhAg \quad (4)$$

Since $[(napy)Cu_2(Ph)]^+$, $[(napy)Ag_2(Ph)]^+$ and $[(napy)CuAg(Ph)]^+$ can be formed via either decarboxylation or desulfination, we examined the CID spectra from both precursors (Figure 3). The CID spectra of $[(napy)Cu_2(Ph)]^+$ are essentially identical (Figures 3A and D), and are dominated by the formation of $[(napy)Cu]^+$ (*m/z* 193) via loss of phenyl copper (eq. 5). The water adducts $[(napy)Cu(H_2O)]^+$ (*m/z* 211) are formed via the reaction of $[(napy)Cu]^+$ with adventitious water present in the ion-trap (eq. 6). $[(napy)Ag_2(Ph)]^+$ fragments solely via loss of phenyl silver (eq. 5). $[(napy)CuAg(Ph)]^+$ fragments via the competitive losses of phenyl copper (eq. 7a) and phenyl silver (eq. 7b), with the former being favored, consistent with DFT calculations of the relative energies for eqs **7a (**ΔE = 69.1 kcal/mol) and **7b (**ΔE = 71.5 kcal/mol**)**.

$$[(napy)M_2(Ph)]^+ \rightarrow [(napy)M]^+ + PhM \quad (5)$$

$$[(napy)Cu]^+ + H_2O \rightarrow [(napy)Cu(H_2O)]^+ \quad (6)$$

$$[(napy)CuAg(Ph)]^+ \rightarrow [(napy)Ag]^+ + PhCu \quad (7a)$$

$$\rightarrow [(napy)Cu]^+ + PhAg \quad (7b)$$

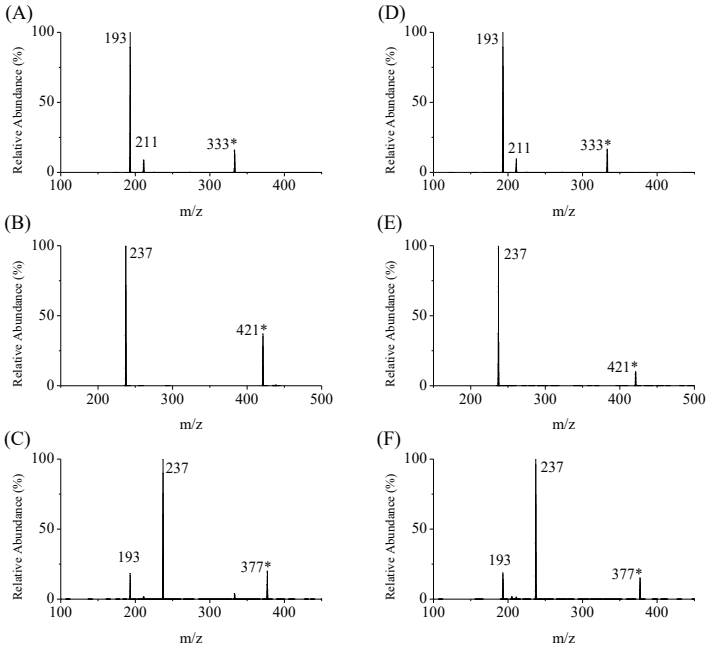

Figure 3: LTQ low energy CID MS^3 mass spectra obtained using a Q value of 0.25 and an activation time of 30 ms with the given normalized collision energies (NCE) for the following species: **(A)** $[(napy)Cu_2(Ph)]^+$ (**10a** *m/z* 333, NCE = 18%) formed via decarboxylation of $[(napy)Cu_2(O_2CPh)]^+$ (**7a**); **(B)** $[(napy)Ag_2(Ph)]^+$ (**10b** *m/z* 421, NCE = 10%) formed via decarboxylation of $[(napy)Ag_2(O_2CPh)]^+$ (**7b**); **(C)** $[(napy)CuAg(Ph)]^+$ (**10c** *m/z* 377, NCE = 13%) formed via decarboxylation of $[(napy)CuAg(O_2CPh)]^+$ (**7c**); **(D)** $[(napy)Cu_2(Ph)]^+$ (**10a** *m/z* 333, NCE = 18%) formed via desulfination of $[(napy)Cu_2(O_2SPh)]^+$ (**7d**); **(E)** $[(napy)Ag_2(Ph)]^+$ (**10b** *m/z* 421, NCE = 11%) formed via desulfination of $[(napy)Ag_2(O_2SPh)]^+$ (**7e**); **(F)** $[(napy)CuAg(Ph)]^+$ (**10c** *m/z* 377, NCE = 13%) formed via desulfination of $[(napy)CuAg(O_2SPh)]^+$ (**7f**). * represents the monoisotopic peaks corresponding to ^{63}Cu, ^{107}Ag and ^{32}S isotopes that were mass selected. Spectra were obtained using the LTQ mass spectrometer.

3 DFT calculations on isomeric structures of $[(napy)Cu_2(Ph)]^+$, $[(napy)Ag_2(Ph)]^+$ and $[(napy)CuAg(Ph)]^+$.

Although the crystal structure of **2** (Scheme 1B) [10a] clearly shows that the substituted napy ligand bridges two Cu centers and that the phenyl group binds in a μ-fashion, it is known that napy ligands without additional exocyclic donor groups are labile[38]. Thus, we not only considered structure **10**, but also isomeric structures in which the napy ligand coordinated to only one of the Cu centers (Figure 4). Related isomeric structures were considered for $[(napy)Ag_2(Ph)]^+$ (Figure S1) and $[(napy)CuAg(Ph)]^+$ (Figure S2). **10a** is the most stable isomer, where the two central Cu atoms interact with both the napy and phenyl ligands. The napy ligand is co-planer with the Cu_2 unit in **10a** with a μ, μ-bonding arrangement, which has an angle of nearly 90° perpendicular to the phenyl ring. Isomers **13a** and **14a** are 9.9 and 24.6 kcal/mol higher in energy than **10a**, and both contain a phenyl ligand that bridges the two copper centers, while having the napy ligand coordinated to only one of the copper centers. In **13a** the napy ligand is co-planer

with the Cu_2 unit, while in **14a** it is not. The final isomer located is **15a**, which no longer contains a Cu_2 unit with a μ, μ-bonding arrangement. Instead, one copper center binds to the phenyl ligand via a sigma bond, with its other coordination site taken up by binding to the napy ligand in a monodentate fashion to give a near linear (Ph)C-Cu-N(napy) arrangement ($\angle_{C\text{-}Cu\text{-}N}$ = 177°). The second copper cation binds via μ_5-coordination to the phenyl ring. In the case of $[(napy)Ag_2(Ph)]^+$, apart from **10b**, only the isomers **13b** and **14b** in which the phenyl ligand bridges the two silver centers and the napy ligand coordinate to only one of the silver centers were found. **15b** was not located, with attempts to optimize this structure leading to the formation of **14b**. This suggests that the disilver complex prefers adopting the two-electron three-center bonding in which a stronger Ag-Ag interaction is enhanced by relativistic effects[39]. Isomers **13b** and **14b** are only 0.4 kcal/mol higher in energy than **10b**. A total of 5 isomers were found for $[(napy)CuAg(Ph)]^+$ (Figure S2). Due to the different metal centers (Cu or Ag) coordinating to the napy ligand, four isomers of **10c** were found (**13c**, **14c**, **13c'** and **14c'**). The isomer in which one copper center binds to the phenyl ligand and one silver center coordinates to the napy ligand was located (**15c**), but attempts to optimize a similar isomer in which one silver center binds to the phenyl ligand and one copper center coordinates to the napy ligand resulted in the formation of **14c**. Richard: 10a should have Cu-N lines, and 15a should have Cu-C line(s)

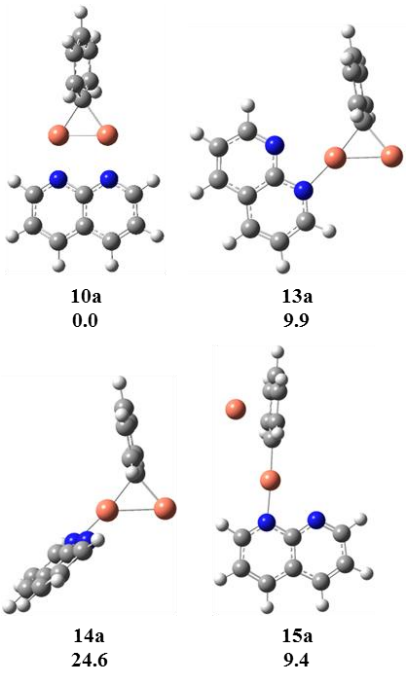

Figure 4: DFT calculated (MO6/SDD6-31G(d)) isomeric structures of $[(napy)Cu_2(Ph)]^+$ showing the different binding arrangements of the napy and phenyl ligands. Relative energies in kcal mol^{-1}. Color codes: Cu (orange), N (blue), C (grey) and H (white).

4 DFT calculations on the formation of $[(napy)Cu_2(Ph)]^+$, $[(napy)Ag_2(Ph)]^+$ and $[(napy)CuAg(Ph)]^+$.

We next used DFT calculations to shed light on the role of the metal centers on the decarboxylation and desulfination reactions of $[(napy)M_aM_b(O_2XPh)]^+$. Based on previous solution phase studies[25], the likely structures of these complexes are **7a-7f** (Scheme 2) and involve μ-binding of both the carboxylate/sulfinate and napy ligands. Consistent with previous calculations for the decarboxylation of a coordinated formate in the binuclear silver complex $[dppmAg_2(O_2CH)]^+$ (dppm = bis(diphenylphosphino)methane)[40], we found that both metal centers were involved in the process of CO_2 extrusion, which involves three steps (Figure 5A). The first step involves breaking one of the Cu-O bonds in **7a-7c** to isomerize the *O,O*- bridged benzoate to its *O*-bound form (**8a** in Figure 5A) via **TS1**. The next step involves breaking the carbon-carbon bond of CuO(O)C-(C_{ipso})Ph, with concomitant formation of a new Cu-C(*ipso*) bond to form the complex **9a** in Figure 5A. **TS2**, which connects the structures **8a** and **9a**, contains an eight-membered ring ($C_{(napy)}$-$N_{(napy)}$-Cu-O-X-C(Ph)-Cu-$N_{(napy)}$). The final step involves barrierless loss of CO_2 from **9a** (Figure S3). A similar mechanism operates for decarboxylation of the binuclear silver cation, $[(napy)Ag_2(O_2CPh)]^+$ (Figure S4). For the heterobinuclear complex, $[(napy)CuAg(O_2CPh)]^+$, phenide transfer from the coordinated benzoate can occur to either metal center. Thus a detailed examination of all possible transition states and intermediates associated with phenide transfer to either copper or silver sites was carried out (Figures S5 and S6). The calculated SO_2 extrusion process from **7d-7f** follows similar pathways (Figure 5) and the structure of all species are given in Figures S7-S10.

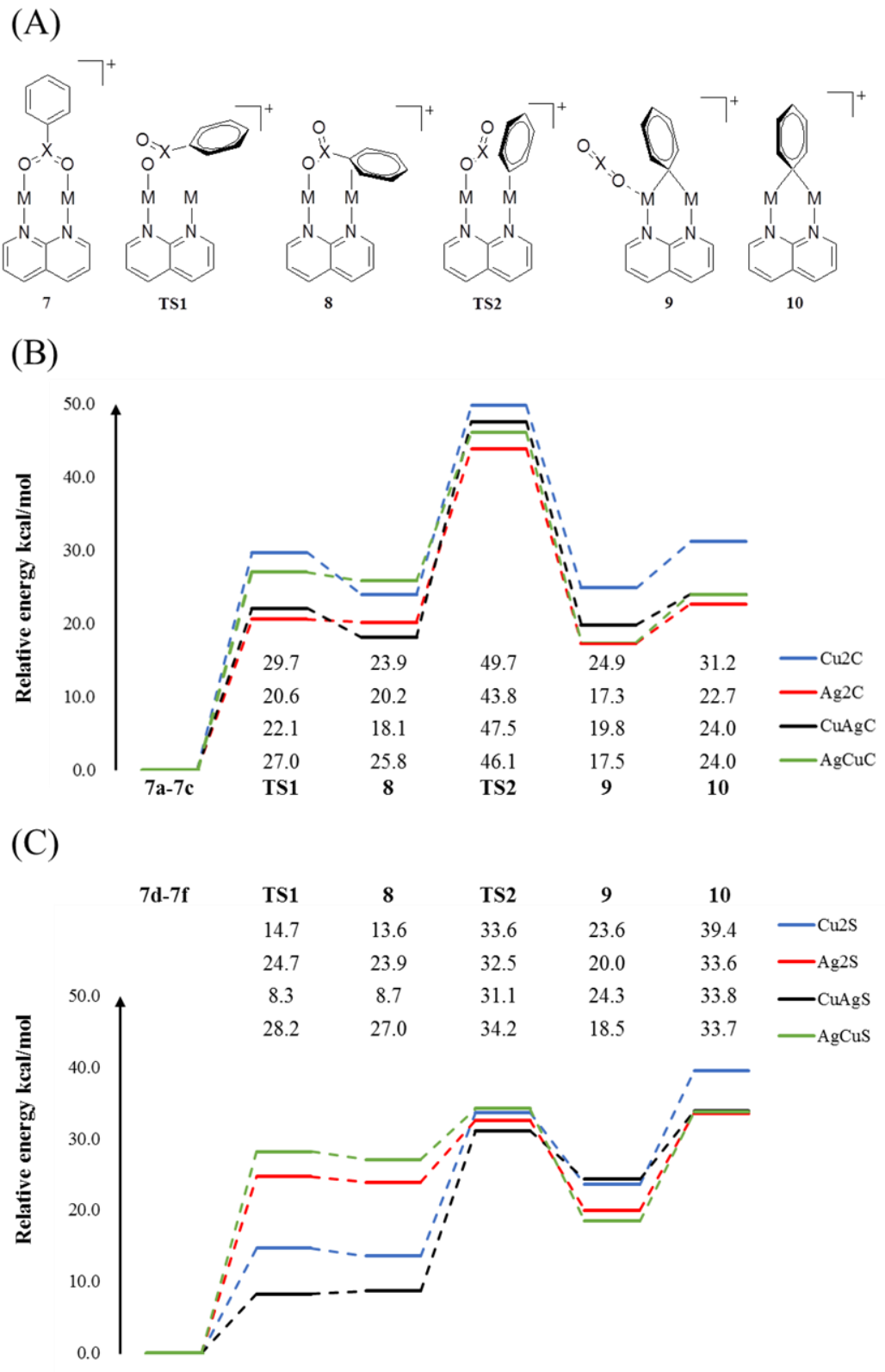

Figure 5: (A) Mechanisms for decarboxylation and desulfination of $[(napy)M_aM_b(O_2XPh)]^+$, X = C or S; DFT calculated (MO6/SDD6-31G(d)) potential energy diagrams for: (B) decarboxylation of $[(napy)M_aM_b(O_2CPh)]^+$ (**7a-7c**); (C) desulfination of $[(napy)M_aM_b(O_2SPh)]^+$ (**7d-7f**). Relative electronic energies in kcal mol^{-1}.

The calculated reaction thermodynamics for decarboxylation and desulfination are given in Figures 5B and C respectively, while Table 1 compares the experimentally determined branching ratios with the DFT calculated energetics for fragmentation via both eqs 1 and 2. Since the temperatures at which fragmentation occurs under the low energy CID conditions of the ion trap are unknown, ΔH and ΔG were not calculated and only the ΔE are given. In all cases the most energetically demanding (rate-determining) step for the extrusion of CO_2 or SO_2 is associated with **TS2** (Figures 5B and 5C). Also noteworthy is that the barriers for desulfination are lower than those for decarboxylation, consistent with the CID experiments, highlighting that loss of SO_2 is kinetically favored. We next describe individual aspects of the decarboxylation and desulfination reactions separately.

Table 1. Relative intensities of fragmentation products (branching ratios, BR) and relevant calculated energies of the associated pathways for fragmentation of **7a-7f** via decarboxylation/desulfination (eq. 1, Scheme 2), versus metal carboxylate/sulfinate loss (eq. 2, Scheme 2).

Precursor ion	**$[(napy)M_aM_b(Ph)]^+$ + XO_2 (eq. 1)**		**$[(napy)M_a]^+$ + $PhXO_2M_b$ (eq. 2a)[c]**		**$[(napy)M_b]^+$ + $PhXO_2M_a$ (eq. 2b)[c]**	
	BR[a]	E(kcal/mol)[b]	BR[a]	E(kcal/mol)[b]	BR[a]	E(kcal/mol)[b]
$[(napy)Cu_2(O_2CPh)]^+$	97.9%	49.7 (31.2)	2.1%	84.3	n/a	n/a
$[(napy)Ag_2(O_2CPh)]^+$	0.7%	43.8 (22.7)	n/a	n/a	99.3%	53.9
$[(napy)CuAg(O_2CPh)]^+$	68.7%	46.1[d] (24.0)	6.7%	70.1	24.6%	67.7
$[(napy)Cu_2(O_2SPh)]^+$	99.7%	33.6 (39.4)	0.3%	84.1	n/a	n/a
$[(napy)Ag_2(O_2SPh)]^+$	99.5%	32.5 (33.6)	n/a	n/a	0.5%	56.3
$[(napy)CuAg(O_2SPh)]^+$	95.8%	31.1[e] (33.8)	0.5%	71.5	4.0%	69.1

[a] Branching ratios are calculated as the intensity of a fragmentation product divided by the sum of the intensities of all fragmentation products formed via eqs. 1 and 2 multiplied by 100%. [b] DFT-calculated activation energies for **TS2**, which is the rate determining step (and reaction energies in brackets). Energies were calculated at M06/SDD-6-31+G*. [c] The reaction is assumed to be barrierless. [d] Lowest energy **TS2** is for decarboxylation at Ag. [e] Lowest energy **TS2** is for desulfination at CuAg.

The first step for the decarboxylation reaction involves breakage of an oxygen-metal bond of (OC)O-M(M(napy)) via **TS1**, which is more facile for $[(napy)Ag_2(O_2CPh)]^+$ and $[(napy)CuAg(O_2CPh)]^+$ compared to $[(napy)AgCu(O_2CPh)]^+$ and $[(napy)Cu_2(O_2CPh)]^+$. This can be attributed to the weaker Ag-O bond[41]. The second step involves the extrusion of CO_2 from **8** to form **9** via **TS2**. While the barriers for decarboxylation (**TS2a** 49.7kcal/mol > **TS2c** 46.1 kcal/mol > **TS2b** 43.8 kcal/mol) are inversely related to the ease of fragmentation found from CID MS of **7** ($[(napy)Ag_2(O_2CPh)]^+$ > $[(napy)CuAg(O_2CPh)]^+$ >

[(napy)$Cu_2(O_2CPh)]^+$), it is worth noting that decarboxylation is not always the major pathway observed experimentally. Thus, although [(napy)$Ag_2(O_2CPh)]^+$ is predicted to have the lowest barriers for both **TS1** (20.6 kcal/mol) and **TS2** (43.8 kcal/mol), decarboxylation is experimentally observed to be the minor pathway. The reason for this is that the competing fragmentation pathway via metal benzoate loss (eq. 2, Scheme 2) has the lowest DFT predicted energies of all the [(napy)$M_aM_b(O_2CPh)]^+$ systems studied (Table 1, eqs. 2a and 2b). As the predicted energies for metal benzoate loss increases, the branching ratio for this reaction decreases.

The energy resolved CID experiments revealed that the ease of fragmentation for [(napy)$M_aM_b(O_2SPh)]^+$ is less influenced by the nature of the metals (Figures 2D, E and F), [(napy)$Cu_2(O_2SPh)]^+$ (0.0124V) ≈ [(napy)$Ag_2(O_2SPh)]^+$ (0.0126V) ≈ [(napy)$CuAg(O_2SPh)]^+$ (0.0130V). This is consistent with the fact that differences in the energies associated with **TS2** for desulfination are smaller than those for decarboxylation.

5 Gas-phase ion-molecule reactions of [(napy)$M_aM_b(Ph)]^+$ with H_2O

The acid-base chemistry of organometallic compounds continues to attract attention within the context of catalysis[42] and from the fundamental aspect of their stability with respect to hydrolysis. Thus, we next examined the reactivity of the organometallic cations [(napy)$M_aM_b(Ph)]^+$ with water, which was introduced in the modified ion trap mass spectrometer (Figure 6).

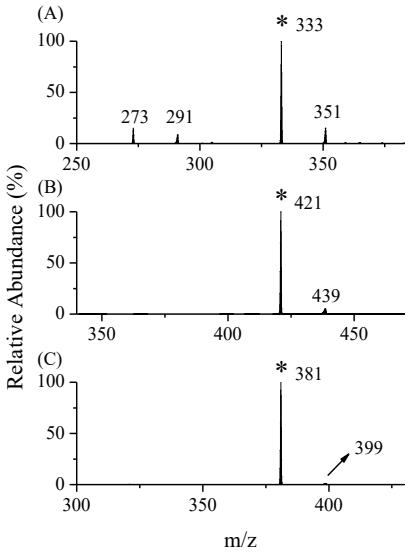

Figure 6: LTQ MS^3 spectra showing ion-molecule reactions between water and the mass selected organometallic cations: (A) [(napy)$^{63}Cu_2(Ph)]^+$ (*m/z* 333); (B) [(napy)$^{107}Ag_2(Ph)]^+$ (*m/z* 421); (C) [(napy)$^{65}Cu^{109}Ag(Ph)]^+$ (*m/z* 381); * represents the monoisotopic peaks that were mass selected. In all

cases, the reaction time was 2 seconds and the concentration of added water was 1.04 x 10^{10} molecules cm^{-3}.

With regards to the depletion of the precursor ion, a relative reactivity order of $[(napy)Cu_2(Ph)]^+$ > $[(napy)Ag_2(Ph)]^+$ > $[(napy)AgCu(Ph)]^+$ was found. $[(napy)Ag_2(Ph)]^+$ and $[(napy)AgCu(Ph)]^+$ solely react to give very minor amounts of adduct ions, which are likely formed via stabilization of the energized adducts formed in eq. 8 by collisions with the helium bath gas (eq. 9) and the rates of these reactions were too slow to measure. $[(napy)Cu_2(Ph)]^+$ reacts with water at a rate of 2.4 x 10^{-11} cm^3 $molecules^{-1}$ s^{-1} corresponding to a reaction efficiency of add value here. The following three product ions are observed (Figure 6(a)): the adduct $[(napy)Cu_2(Ph)(H_2O)]^+$ (*m/z* 351, eqs. 8 and 9), the hydrolysis product $[(napy)Cu_2(OH)]^+$ (*m/z* 273, eq. 10), and $[(napy)Cu_2(OH)(H_2O)]^+$ (*m/z* 291). The latter ion is the product of a secondary reaction between $[(napy)Cu_2(OH)]^+$ and water (eq. 11).

$$[(napy)M_aM_b(Ph)]^+ + H_2O \rightarrow [(napy)M_aM_b(Ph)(H_2O)]^{+*} \quad (8)$$

$$[(napy)M_aM_b(Ph)(H_2O)]^{+*} + He \rightarrow [(napy)M_aM_b(Ph)(H_2O)]^+ + He \quad (9)$$

$$[(napy)Cu_2(Ph)]^+ + H_2O \rightarrow [(napy)Cu_2(OH)]^+ + C_6H_6 \quad (10)$$

$$[(napy)Cu_2(OH)]^+ + H_2O \rightarrow [(napy)Cu_2(OH)(H_2O)]^+ \quad (11)$$

The yields of the adduct ions $[(napy)Cu_2(Ph)(H_2O)]^+$ and $[(napy)Ag_2(Ph)(H_2O)]^+$ were sufficient for them to be mass selected and subjected to CID (Figure 7). $[(napy)Cu_2(Ph)(H_2O)]^+$ fragments via loss of benzene to give the hydrolysis product $[(napy)Cu_2(OH)]^+$ (eq. 12a), suggesting that the barrier is lower than the energy required to lose water to regenerate the organometallic cation $[(napy)Cu_2(Ph)]^+$ via eq. 12b. In contrast, $[(napy)Ag_2(Ph)(H_2O)]^+$ fragments to regenerate the organometallic cation $[(napy)Ag_2(Ph)]^+$ (eq. 12b).

$$[(napy)M_aM_b(Ph)(H_2O)]^+ \rightarrow [(napy)M_aM_b(OH)]^+ + C_6H_6 \quad (12a)$$

$$\rightarrow [(napy)M_aM_b(Ph)]^+ + H_2O \quad (12b)$$

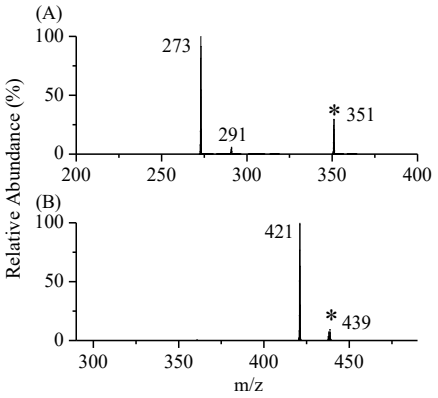

Figure 7: LTQ MS^4 spectra showing the CID products of: (A) $[(napy)Cu_2(Ph)(H_2O)]^+$ (*m/z* 351); and (B) $[(napy)Ag_2(Ph)(H_2O)]^+$ (*m/z* 439). * represents the monoisotopic peaks corresponding to ^{63}Cu and ^{107}Ag isotopes that were mass selected.

6 DFT calculations on the reactions of $[(napy)Cu_2(Ph)]^+$, $[(napy)Ag_2(Ph)]^+$ and $[(napy)AgCu(Ph)]^+$ with water.

To gain further insights into the experimentally observed relative reactivity orders for the reactions of $[(napy)M_aM_b(Ph)]^+$ and H_2O, DFT calculations were carried out to determine the structures and energetics of the reactants, intermediates, products and transition states. We found that the potential energy diagrams not only follow the classical Brauman double well[43] (Figure 8), but also are very similar to a reverse reaction of C-H activation of C_6F_5H and 2-methylthiophene at a binuclear silver center, utilizing pivalic acid in place of water[44]. Thus, approach by the water molecule to the organometallic cations is barrierless and gives rise to the isomeric adducts $[(napy)M_aM_b(Ph)(H_2O)]^+$, **17** and **17'**. In these adducts **17**, the oxygen of H_2O is bound to one metal center, M_a of $[(napy)M_aM_b(Ph)]^+$, where the M_a-N bond is substantially elongated (Supporting Information Figures S12-S15). In adducts **17'**, the bound H_2O does not have a strong effect on the M_a-N bond, which is 2.05 Å in **17a'** while 1.99 Å in **10a**. With the re-installation of the M_a-N bond, the phenyl group becomes close to the H_2O molecule on the M_a atom. This has essentially led to a favorable geometric configuration where one H atom of H_2O interacts with the α-carbon of the phenyl group in **TS3**. Based on potential energy scans, there appears to be no barrier for interconversion of **17** and **17'** (Supporting Information Figure S11). **TS3**, in which the coordinated H_2O is deprotonated by the coordinated phenyl anion via a O(H)H-C(Ph) interaction, is formed from adduct **17'**. The product complexes $[(napy)M_aM_b(OH)(C_6H_6)]^+$, **18** then fragment via barrierless loss of benzene.

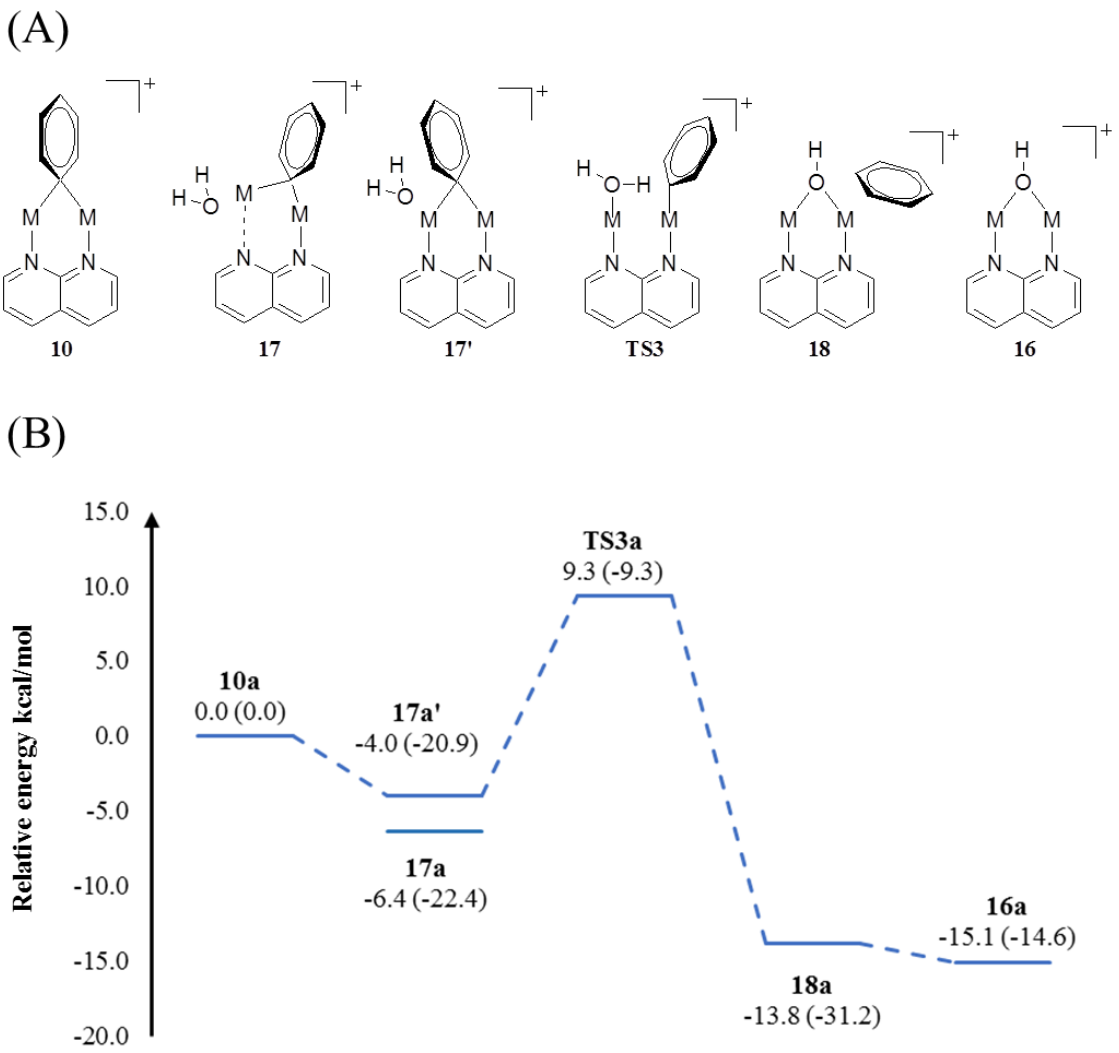

Figure 8: DFT calculated (MO6/SDD6-31G(d)) reaction pathway for the ion-molecule reaction of $[(napy)M_aM_b(Ph)]^+$ with water: (A) key species associated with the hydrolysis mechanism; (B) potential energy diagrams for the reactions of: $[(napy)Cu_2(Ph)]^+$ (**10a**). The relative Gibbs and enthalpy energies (in parentheses) are given in kcal mol^{-1}. (Richard: normally I would have shown a dotted line for M…O in **17** and **17'**, O…H…Cipso for **TS3** since O-H is weakening, and any short M…C distance(s) for **18**)

The calculated energetics shown in Figure 8B (Supporting Information, Figures S13 and S14) are consistent with the experimentally observed reactivity. Thus for $[(napy)Cu_2(Ph)]^+$, the only cation to undergo hydrolysis, not only is the barrier height the lowest (-9.3 kcal/mol) relative to the separated reactants, but the overall reaction is the most exothermic (-14.6 kcal/mol). The calculated Gibbs energy changes showed

the same trend that $[(napy)Cu_2(Ph)]^+$ has the lowest activation barrier of 9.3 kcal/mol and an enthalpy of -15.1 kcal/mol.

Conclusion

There is continued interest in the synergistic effect of two metal centers on reactivity[40,45]. We have found that the type of metal centers in $[(napy)M_aM_b(O_2XPh)]^+$ and $[(napy)M_aM_b(Ph)]^+$ systems influences their reactivity. Thus the branching ratios for formation of $[(napy)M_aM_b(Ph)]^+$ are the highest for both the homonuclear copper carboxylate and sulfinate complexes, and only $[(napy)Cu_2(Ph)]^+$ undergoes hydrolysis. Futhermore, the DFT calculations show that both metal centers play a role in decarboxylation and desulfination of $[(napy)M_aM_b(O_2XPh)]^+$ and in the ion-molecule reactions of $[(napy)M_aM_b(Ph)]^+$ with water. Thus one metal site acts as an "anchor" for the oxygen of the carboxylate or sulfinate (Figure 5) or the water (Figure 8) while the other site either accepts the migrating phenide during decarboxylation or desulfination (**TS2**) or faciltates deprotonation of water by the coordinated phenide in the hydrolysis step (**TS3**). Further studies are underway to examine synergistic effects in the reactivity of ligated dimetallated organometallic complexes.

Experimental

Reagents

All chemicals were used without further purification: copper(I) acetate and benzenesulfinic acid sodium salt from Aldrich; silver nitrate and methanol (AR grade) from Chem-Supply; benzoic acid from May & Baker; 1.8-naphthyridine (napy) from Matrix Scientific and acetic acid from BDH chemicals.

Mass spectrometry experiments

Mass spectrometry experiments were carried out on a Thermo Scientific (Bremen, Germany) LTQ FT hybrid mass spectrometer equipped with a Finnigan electrospray ionization source and modified to allow the study of ion-molecule reactions[46]. Under ion-molecule reaction conditions, collisions with the helium bath gas quasi-thermalize the ions to room temperature.[47]

Gas-phase formation of $[(napy)M_aM_b(O_2CPh)]^+$ (7a-7c)

Copper(I) acetate was dissolved in methanol with acetic acid in a 2:3 molar ratio. Silver nitrate was dissolved in methanol. Methanolic solutions of metal salts were added to a mixture of 1.8-naphthyridine (napy) and benzoic acid and then diluted to a 0.5 mM methanol solution in a 1:2:1 molar ratio (for 1c the ratio is 1:1:2:1 copper(I) acetate/silver nitrate/napy/benzoic acid). The diluted solutions were injected at a flow rate of 5 μL min^{-1} into the ESI source. Typical ESI source conditions involved: needle potentials = 3.5-4.5 kV, capillary temperature = 250 °C, nitrogen sheath gas pressure = 10-20 arbitrary units, capillary voltage = -0.40-50V, tube lens voltage = 15-225V. The binuclear coordinated benzoates $[(napy)M_aM_b(O_2CPh)]^+$ (**7a-7c)** were examined via low-energy collision-induced dissociation (CID). CID experiments were carried out by mass selecting the single isotope cluster with a window of 1 m/z and applying a normalized collision energy between 8% and 20% to allow collisions with the helium bath gas. An activation Q value of 0.25 and an activation time of 30 ms were used.

Gas-phase formation of $[(napy)M_aM_b(O_2SPh)]^+$ (7d-7f)

Methanolic solutions of metal salts were added to a mixture of 1.8-naphthyridine (napy) and benzenesulfinic acid sodium salt and then diluted to a 0.5 mM methanol solution in a 1:2:1 molar ratio (for 1f the ratio is 1:1:2:1 copper(I) acetate/silver nitrate/napy/benzoic acid). The diluted solutions were injected at a flow rate of 5 μL min^{-1} into the ESI source. Typical ESI source conditions involved: needle potentials = 3.6-4.2 kV, capillary temperature = 250 °C, nitrogen sheath gas pressure = 20 arbitrary units, capillary voltage = 15-50V, tube lens voltage = 60-160V. The ligated binuclear cations $[(napy)M_aM_b(O_2SPh)]^+$ (**7d-7f)** were examined via low-energy collision-induced dissociation. CID experiments were carried out by mass selecting the single isotope cluster with a window of 1 m/z and applying a normalized collision energy between 8% and 20% to allow collisions with the helium bath gas. An activation Q value of 0.25 and an activation time of 30 ms were used.

Energy resolved CID

We assessed the relative decarboxylation of $[(napy)M_aM_b(O_2CPh)]^+$ (**7a-7c**) and desulfination of $[(napy)M_aM_b(O_2SPh)]^+$ (**7d-7f**), respectively, via energy-resolved CID studies, which were undertaken on the LTQ mass spectrometer as described by Colorado and Brodbelt[33]. These experiments measure the decrease in the intensity of the precursor ion and the appearance and intensity of fragmentation products as the collision energy is increased in a step-wise fashion. The normalized collision energy (NCE), which sets the amplitude of the RF energy applied to the end-cap electrodes, was converted to its laboratory frame applied voltage. The following experimental parameters were used: (a) a Q of 0.25 was used; (b) an activation time of 10 ms was selected throughout the ERCID experiment; (c) the monoisotopic peaks for **7a-7c** and **7d-7f** were mass selected with a 1-1.5 m/z window for single isotopes of ^{63}Cu, ^{107}Ag and

^{32}S. The "threshold voltage" was defined as the voltage at which the parent ion intensity was 50% of the total ion intensity.

CID of $[(napy)M_aM_b(Ph)]^+$ (10a-10c)

Typical ESI source conditions involved: needle potentials = 4.5-4.6 kV, capillary temperature = 250 °C, nitrogen sheath gas pressure = 10 arbitrary units, capillary voltage = 0-50V, tube lens voltage = 20-230V. The ligated binuclear cations $[(napy)M_aM_b(Ph)]^+$ (**10a-10c)** formed via decarboxylation and desulfination were examined via low-energy collision-induced dissociation. CID experiments were carried out by mass selecting the single isotope cluster with a window of 1 m/z and applying a normalized collision energy between 10% and 18% to allow collisions with the helium bath gas. An activation Q value of 0.25 and an activation time of 30 ms were used.

IMR of $[(napy)M_aM_b(Ph)]^+$ (10a-10c) with H_2O

H_2O was heated to the boiling point and then injected to the helium bath gas to introduce into the ion trap of a modified LTQ mass spectrometer to allow IMR experiments. Monoisotopic peaks were mass-selected and allowed to react with H_2O in the ion trap and the activation time was varied between 2000ms and 10000ms. Because H_2O was in great excess in the ion trap, the concentration of H_2O was considered constant and determined by the neutral flow rate and helium flow rate.

Computational details

Gaussian 09 [48] was used to fully optimize all the structures reported in this paper at the M06 level of density functional theory (DFT) [49]. The Stuttgart Dresden (SDD) basis set was used for copper and silver atoms.[50] The 6-31G(d) basis set was used for other atoms.[51] Frequency calculations were carried out at the same level of theory as those for the structural optimization. Transition structures were located using the quadratic synchronous transit approach (QST3).[52] Intrinsic reaction coordinate (IRC) calculations were carried out to confirm that reactant and product minima connected to the transition state.[53]

Supporting Information

Additional structural pictures of the DFT optimized structures, the charts of potential energy surface scan and Cartesian coordinates (PDF)

Statement: The authors declare no competing financial interests.

ORCID
Jiaye Li: 0000-0002-5071-5325
Richard O'Hair: 0000-0002-8044-0502
Allan Canty: 0000-0003-4091-6040

ACKNOWLEDGMENT

We thank the Australian Research Council for financial support DP150101388 and DP180101187 (to RAJO and AJC). The authors gratefully acknowledge the generous allocation of computing time from the University of Tasmania and the National Computing Infrastructure (fz2 and zg2).